Realization of ideal nodal-line fermions in doped Ni_3In-based structures

Ye Yang,[1] Rui Wang,[2,*] and Xianhui Chen[1,3,†]
[1]*Department of Physics, and CAS Key Laboratory of Strongly-Coupled Quantum Matter Physics, University of Science and Technology of China, Hefei, Anhui 230026, China*
[2]*Institute for Structure and Function, Department of Physics, and Center for Quantum Materials and Devices, Chongqing University, Chongqing 400044, China*
[3]*CAS Center for Excellence in Quantum Information and Quantum Physics, Hefei, Anhui 230026, China and Collaborative Innovation Center of Advanced Microstructures, Nanjing 210093, China*

(Received 28 August 2023; revised 11 January 2024; accepted 3 April 2024; published 1 May 2024)

The discovery of the ideal topological semimetallic state in experimentally accessible materials is of both fundamental and technological interest. Here, based on first-principles calculations using the virtual crystal approximation method, we study the evolution of band structures in the Ni_3In cubic structure by intercalating the doped C or N atoms, termed as $Ni_3InC_xN_{(1-x)}$. Through controlling the ratio of intercalated atoms, we calculate electronic structures of a series of doped samples. A distinctive feature of a nodal line occurring at the Fermi level is present at $x = 0.26$, and the charge analysis indicates that the bond interaction between intercalated atoms and nickel atoms induces charge redistribution, giving rise to the rigidlike shift of bands. Within the spin-orbital coupling, the nodal line is gapped and thereby $Ni_3InC_xN_{(1-x)}$ transforms into topological insulators due to the spin-rotation symmetry breaking. Moreover, the nontrivial state is insensitive to the external strain and pressure, so one can expect exotic correlation physics of massless nodal-line fermions in the doped systems of $Ni_3InC_xN_{(1-x)}$. Our work provides a promising avenue to explore ideal topological massless quasiparticles in doped systems.

DOI: 10.1103/PhysRevB.109.205103

I. INTRODUCTION

Over the past decade, one of the emerging topics in condensed matter physics is the exploration of topological semimetals (TSMs) with band structures protected by the interplay of symmetry and topology [1–13]. Compared to ordinary three-dimensional (3D) metals in which the filled and empty states are separated by two-dimensional (2D) Fermi sheets, 3D TSMs exhibit zero-dimensional (0D) discrete nodal points or one-dimensional (1D) continuous nodal lines, such as Weyl semimetals, Dirac semimetals, nodal-line semimetals (NLSMs), and others [9,13–16]. Among various TSMs, NLSMs, which possess 1D Fermi surfaces accompanied by drumhead surface states, are of particular interest. The weakly dispersing drumhead surface states of NLSMs can provide an interesting platform for exotic correlation physics of massless quasiparticles [17–21], and thus NLSMs have been drawing intense attention. Recently, the topological gapless modes of NLSMs have been demonstrated to support unusual transport properties [22–27].

Up to now, there have been several theoretical proposals and a few experimental observations for material realization of NLSMs [7–11,28–32]. Unlike Weyl semimetals, the stability of a NLSM requires symmetry, which may be the combination of inversion and time-reversal symmetry, a mirror reflection symmetry, or a nonsymmorphic symmetry [14,15]. From the topological viewpoint, these symmetries can quantize the Berry phase for a continuous band along a circle in the momentum space [14]. In this case, valence bands inside and outside a nodal line have opposite eigenvalues of symmetry operators. For NLSMs protected by inversion (I) and time-reversal (T) symmetries, the spin-rotation symmetry enables us to effectively treat electrons as spinless fermions with $(IT)^2 = 1$ [8,33]. This kind of nodal line can be gapped by spin-orbital coupling (SOC), since the SOC effect breaks the spin-rotation symmetry, making the symmetry protection of the topological charge ineffective. Representative materials of this type of band crossing are Cu_3NZn and Cu_3NPd [8,28]. In these materials, the intercalation of a transition metal atom at the body center of the cubic unit cell Cu_3N in an antiperovskite structure is crucial for realizing nodal lines. Owing to its high symmetry, the antiperovskite structure possesses a distinct advantage in forming nodal lines that are protected by the combination of inversion and time-reversal symmetries. In addition, importantly, the symmetry of the A_3B cubic structure remains upon the introduction of an intercalated atom at its body center. Thus, by controlling the types of intercalated atoms, it is expected to realize the conduction band and valence band accurately crossing at the Fermi level. It is worth noting that nodal lines constrained to occur at zero energy in the context of models usually require an additional chiral symmetry [34]. However, chiral symmetry is a hypothetical concept for the band structure of a realistic material. Therefore, the presence of ideal nodal lines at the Fermi level via tuning chemical compositions is significant and experimentally accessible.

*rcwang@cqu.edu.cn
†chenxh@ustc.edu.cn

In this work, based on first-principles calculations using the virtual crystal approximation (VCA) method to mimic the doping effect, we study the evolution of band structures and the realization of ideal nodal lines in doped Ni_3In cubic structures. By controlling the proper ratio of intercalated C or N atoms at the body-center position, we obtain a series of electronic structures of doped samples of $Ni_3InC_xN_{(1-x)}$ for different x values. We find that the evolution of the electronic band structure can be described by a rigidlike shift, which is similar to hole or electron doping. Remarkably, when $x = 0.26$, the conduction band and valence band cross at the Fermi level, forming ideal nodal lines around the high-symmetry point M in the first Brillouin zone (BZ). The other set of nodal lines encircling around the high-symmetry point X is also present. All the nodal lines are protected by the combination of inversion and time-reversal symmetry. Employing topology and charge analysis, the presence of nodal lines is associated with the chemical potential changing induced by charge redistribution. When SOC is present, the broken spin-rotation symmetry drives the nodal lines to be gapped. Moreover, the nontrivial state in $Ni_3InC_xN_{(1-x)}$ is less sensitive to the external strain and pressure, so the exotic correlation physics of massless nodal-line fermions could be expected to emerge in these doped systems.

II. COMPUTATIONAL METHODS

On the basis of density functional theory (DFT) [35], we employed the Vienna *ab initio* simulation package (VASP) [36] to obtain the electronic structures. The Perdew-Burke-Ernzerhof (PBE) functional [37] can describe electronic exchange correlation interactions. The cutoff energy of the plane-wave-basis was set to 450 eV with a $14 \times 14 \times 14$ Monkhorst-Pack grid in the first Brillouin zone (BZ) [38]. The crystal structures were fully relaxed until the force of each atom was smaller than 10^{-3} eV/Å. We calculated the parity eigenvalues at time-reversal invariant momenta (TRIM) points within the IRVSP package [39] to evaluate the topological properties. Further, we calculated the topological properties using the WANNIER90 [40] and WANNIERTOOLS packages [41]. To evaluate the stability of considered systems, we simulated the phonon dispersion by the finite displacement method based on the PHONOPY package [42]. A $3 \times 3 \times 3$ supercell with $4 \times 4 \times 4$ k mesh is used to calculate the phonon spectrum. Here we use the virtual crystal approximation (VCA) method to calculate electronic structures of doped systems. In the VCA method, the doped effects are modeled by the fictitious atoms occupied at the lattice site via statistical methodology. Therefore, the arrangement of dopant atoms is not being taken into account.

III. RESULTS AND DISCUSSION

As shown in Fig. 1, the Ni_3In compound consists of the nickel atoms locating on the face-center sites and the indium atoms locating on the corner sites. It has a face-centered cubic structure (fcc) with a space group $Pm\bar{3}m$ (No. 221), where the Ni atoms form a kagome plane perpendicular to the [111] direction. In this compound, any of the x, y, and z axes are the twofold, fourfold rotational axes, and mirror reflection M_i ($i = x, y, z$) perpendicular to the x, y, and z axes, respectively. Considering the *Oh* point group, its body diagonals guarantee the possibility of threefold rotation. Introducing an atom in the body-center site can drive the lattice into so-called "antiperovskite structure" A_3BX ($A =$ Ni, $B =$ In, $X =$ C,N). The Ni_3InX contains XNi_6 octahedral structures but retains the symmetry operations of Ni_3In. The intercalated atom occupies the octahedral center site which would induce the charge redistribution in the lattice. Here we propose carbon and nitrogen as the intercalated atom. As illustrated by the electron localization function (ELF) (Fig. S1 in the Supplemental Material [43]), all of the electrons would disperse in the whole lattice which is recognized as a typical metallic bonds characteristic. In contrast, interstitial electrons are highly localized around the C(N) atoms of Ni_3InC (Ni_3InN). Moreover, Ni_3InX ($X =$ C, N) has good thermodynamic stability through the phonon dispersion results shown in Fig. S2 of the Supplemental Material [43].

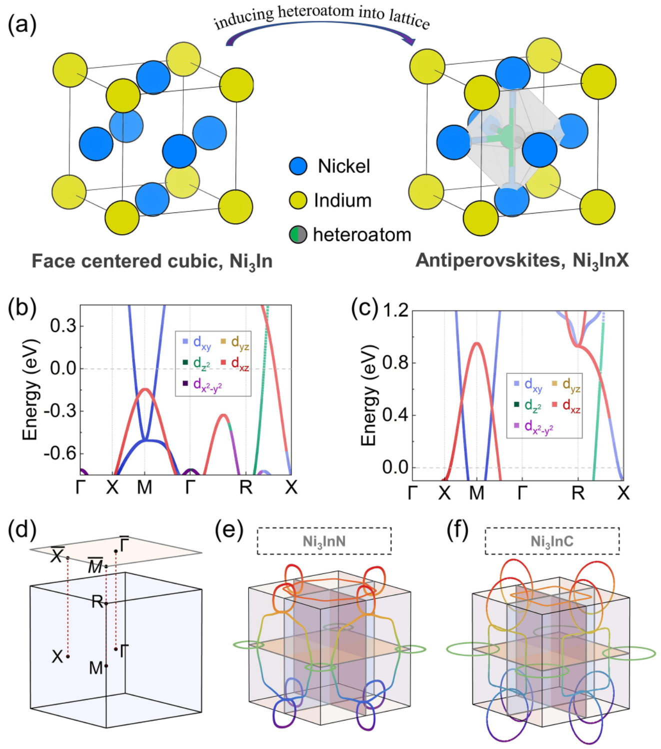

FIG. 1. (a) The crystal structure of Ni_3In and Ni_3InX ($X =$ C, N). (b), (c) The calculated band structure of Ni_3InN and Ni_3InC, respectively. (d) The Brillion zone (BZ) with marked high-symmetry points. (e), (f) the schematic diagram of nodal-line rings in the Ni_3InN and Ni_3InC, respectively.

The influence of charge redistribution can directly reflect on the electronic band structure. For Ni_3In, the bands near the Fermi level are dominated by the Ni $3d$ orbital (see Fig. S3 in the Supplemental Material [43]). Multiple bands couple together to form crossing points near the Fermi level. Given the spin-orbital coupling (SOC), these crossing points would be gapped but metal characteristics remain. With the introduction of a heteroatom, this compound would experience a phase transition from trivial metal to nontrivial semimetal.

As shown in Fig. 1(b), we first calculated the band structures of Ni_3InN without SOC. In this case, we found that

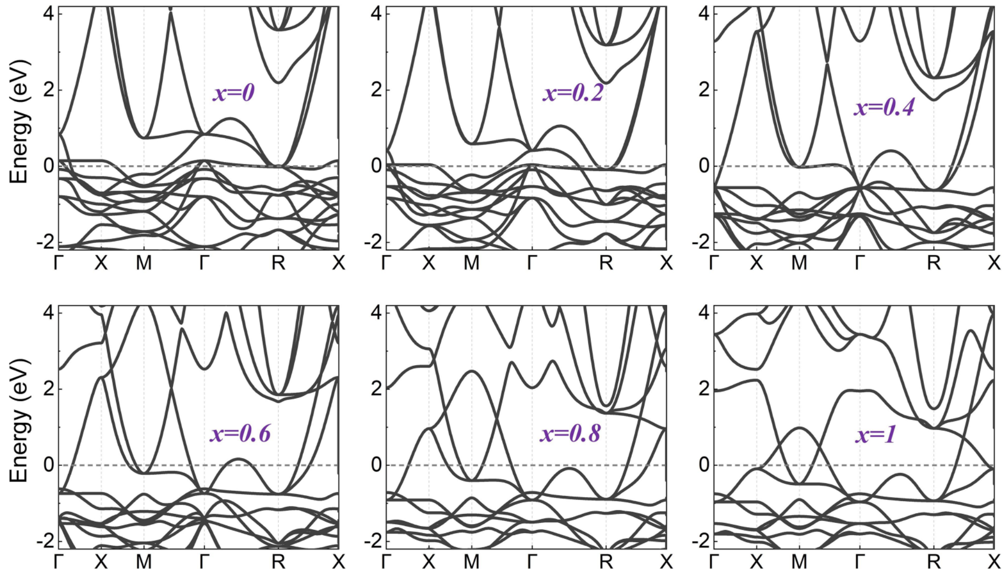

FIG. 2. The band evolution of Ni_3InC_x. With the concentration of the carbon atom in the body-center site increasing, the crossing points around the *M* point would be shifted from the above ∼4 eV to zero energy.

band crossing points along the *X*-*M* and *M*-Γ high-symmetry paths are present, which are about −0.21 eV below the Fermi level. By checking the irreducible representation (IR) of the corresponding bands, the opposite eigenvalues indicates that these points are of symmetry-enforced Dirac points. These Dirac points can form a small circle enclosing the *M* point by analyzing lattice symmetries. Their energies are approximately flat [see Fig. 1(e)]. All the symmetry-protected crossing points can form 12 Dirac nodal lines (DNLs) with respect to the mirror-reflection symmetries in the Brillouin zone. In addition, we emphasize that the band crossing point is also bound to occur in the *R*-*X* high-symmetry path, but is impossible along the Γ-*X* or Γ-*R* high-symmetry paths. As shown in Fig. 1(e), the cubic symmetry guarantees that DNLs encircle the inequivalent *X* points on the three mirror planes, respectively. Briefly, there are two symmetry-enforced categorizations of DNLs: One belongs to nodal rings near the *M* points and the other is DNLs encircling the *X* points. The band structures of Ni_3InC are shown in Fig. 1(c). Without SOC, the inversion between occupied and unoccupied states induces the

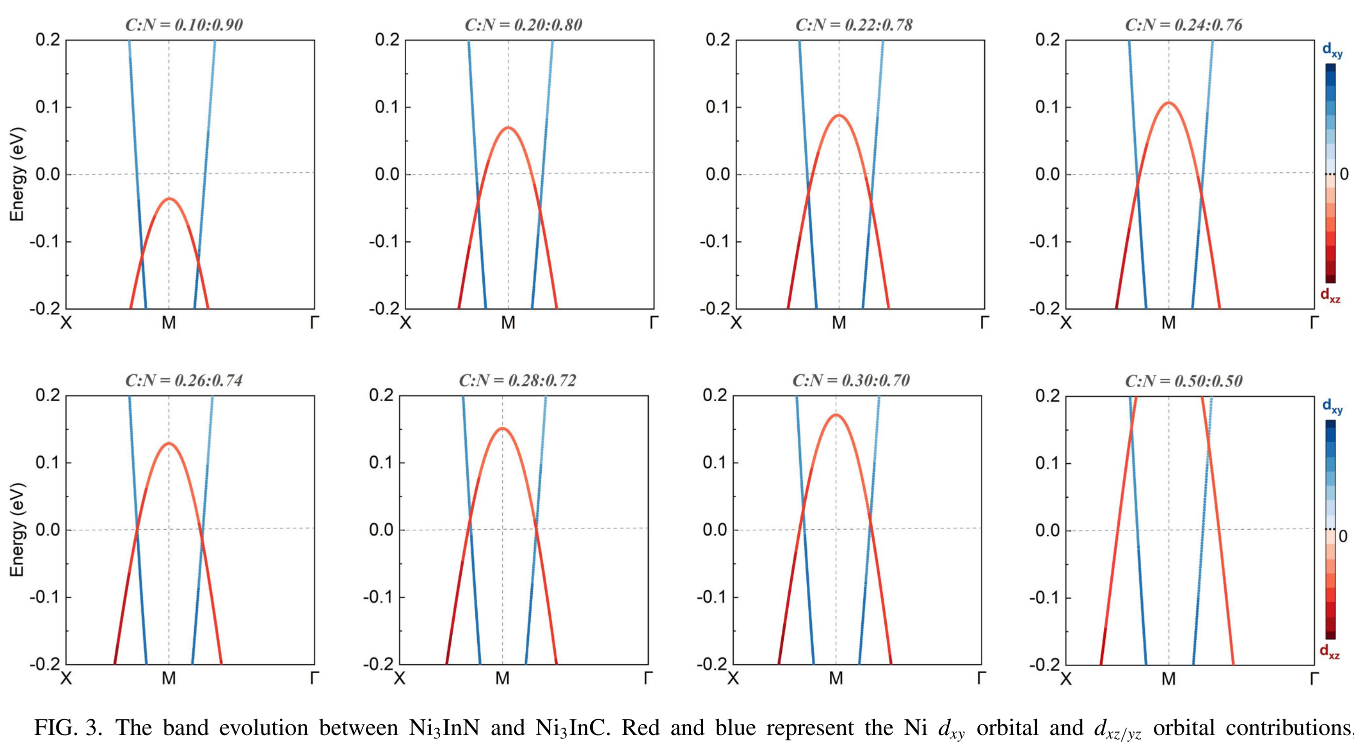

FIG. 3. The band evolution between Ni_3InN and Ni_3InC. Red and blue represent the Ni d_{xy} orbital and $d_{xz/yz}$ orbital contributions, respectively.

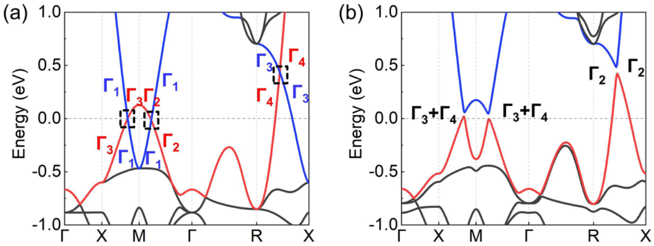

FIG. 4. (a), (b) The calculated band structures of $Ni_3InC_{0.26}N_{0.74}$ with and without SOC, respectively.

fourfold degenerate crossing points to appear along the *X*-*M*, *M*-Γ, and *R*-*X* high-symmetry paths, respectively. As depicted in Fig. 1(f), the locations of nodal rings are the same as the Ni_3InN case.

Based on the above discussion, atom intercalation makes DNLs occur in the vicinity of the Fermi level for such a nonmagnetic cubic system with a frustrated sublattice. To elucidate this topological phase transition mechanism, we employed the virtual crystal approximation (VCA) method to calculate band structure evolution from Ni_3In and Ni_3InC to Ni_3InN. The band evolution from Ni_3In to Ni_3InC is illustrated in Fig. 2. The electronic structures remain essential features but suffer significant effects when a carbon atom is introduced into the body-center site of Ni_3In. The major change is that the NLs above ∼4 eV shift down to the Fermi level. It is mainly contributed from the Ni 3*d* orbital, and the band shift exhibits a rigidlike formalism by the interaction between C and Ni atoms. This result indicates that the intercalated atoms of Ni_3InX only modify the charge distribution rather than induce band renormalization. During the process, there are robust topological features for the critical bands encircling the *X* points and *M* points.

It is worth noting that both pristine Ni_3InN and Ni_3InC exhibit similar nodal crossing behaviors. However, the nodal lines in pristine Ni_3InN and Ni_3InC are far away from the Fermi level. The DNLs of Ni_3InN occur below the Fermi level while for Ni_3InC the DNLs lie above the Fermi level. The question is whether there is any approach to generate ideal DNLs. Taking the *X*-*M*-Γ high-symmetry path as examples, we further calculated the orbital-resolved band evolution between Ni_3InN and Ni_3InC (see Fig. 3). The extra C or N atoms change the electron hopping rules in the lattice, leading to the charge redistributing for Ni 3*d* orbitals. Due to the Ni-C (or Ni-N) bonds in the body-center site, the localized electron density of the d_{xy} and $d_{x^2-y^2}$ orbitals would be increased and that of the d_{z^2}, d_{xz}, and d_{yz} orbitals would be decreased. As shown in Fig. 3, the Dirac points around the *M* point depend on the d_{xy}, d_{xz}, and d_{yz} orbitals. With the ratio of nitrogen increasing, the valence band (d_{xy} orbital) dramatically shifts upward and the conduction band (d_{xz} orbitals) shifts downward, thereby giving rise to the Dirac points moving up gradually in energy. The Dirac point along the *X*-*M* high-symmetry path moves up to the Fermi level once the ratio of C and N reaches 0.26:0.74. The Dirac points along other high-symmetry paths can also be comprehended similarly. These results imply that the charge redistribution induced by atom introducing play an important role in the topological nontrivial state.

As shown in Figs. 4(a) and 4(b), we calculated the band structures of $Ni_3InC_{0.26}N_{0.74}$ without and with SOC, respectively. In the absence of SOC, the Dirac points can locate at the Fermi level along the *X*-*M*-Γ path and ∼0.44 eV above the Fermi level along the *R*-*X* path. The movement of Dirac points on the *R*-*X* high-symmetry path is quicker than that on the *X*-*M*-Γ path. However, only varying the composition of the body-center site itself fails to realize all DNL states with the

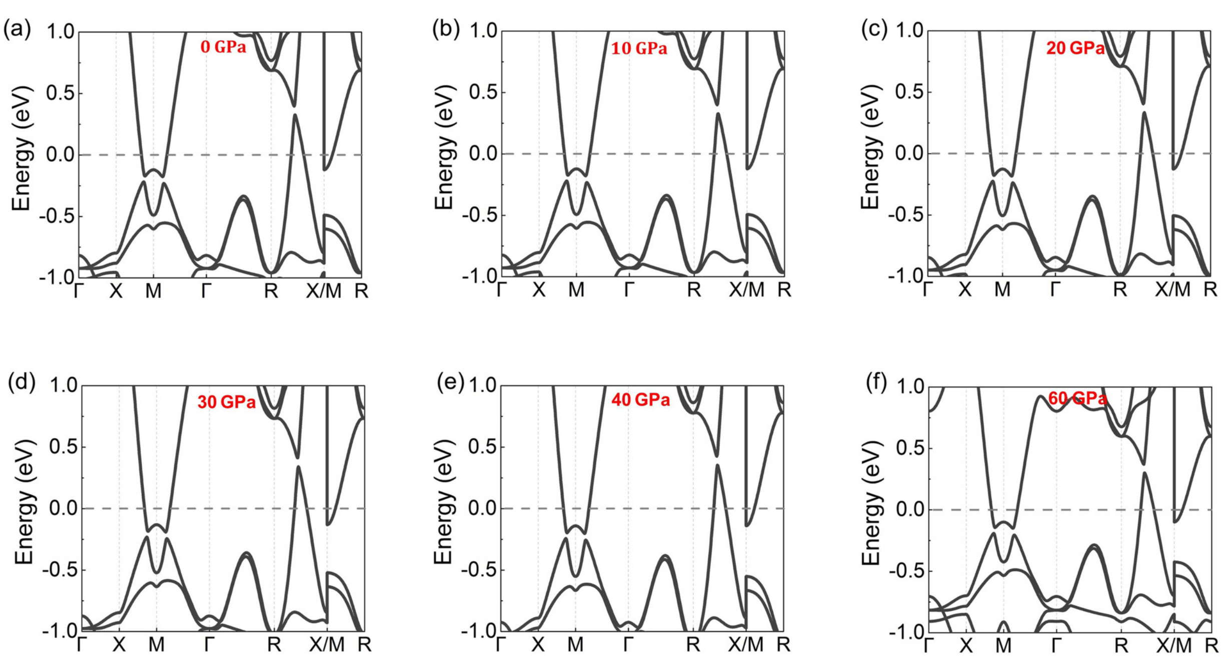

FIG. 5. (a)–(f) The pressure-dependent band structures of Ni_3InN with SOC.

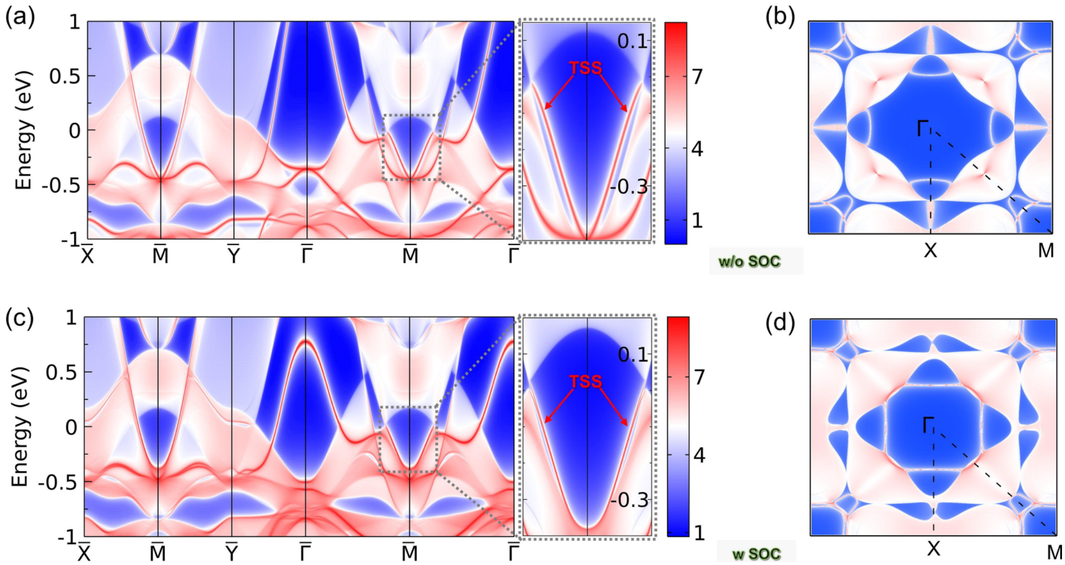

FIG. 6. The projected band structures of $Ni_3InC_{0.26}N_{0.74}$ (a) without SOC and (c) with SOC, respectively. The projected Fermi surface on the (001) surface (b) without SOC and (d) with SOC, respectively. Here, the "TSS" denotes the topological surface state on the (001) surface.

desirable energy simultaneously. As mentioned in previous studies, some approaches like pressure, strain, or charge doping can tune the topological properties of materials [44–48]. As shown in Fig. 5, the crystal volume of Ni_3InN would be smaller with increasing applied pressure, while pressure has negligible influence on the band structure and topological invariant. For other approaches, both Ni_3InN and Ni_3InC also exhibit robust topological features in the range of $\pm 5\%$ strain or certain pressure, as shown in Figs. S4–S6 in the Supplemental Material [43]. Intriguingly, though, the Ni_3InC would be an ideal DNL semimetal candidate while introducing the hole doping. This topological phase can be easily realized in experiments, such as pristine vacancy defect engineering or charge doping by gating, which are both expected to produce exotic transport properties.

In the presence of SOC, the influence of relativistic effects on electronic structures mainly depends on atomic masses and lattice symmetry, so the SOC-induced changes of band structures are relatively weak in materials with light transition-metal elements. When SOC is included, these nodal rings of $Ni_3InC_{0.26}N_{0.74}$ disappear and then finite gaps open due to the broken spin-rotation symmetry. Fortunately, the SOC gaps are 0.04, 0.04, and 0.06 eV along the X-M, M-Γ, and R-X high-symmetry paths, respectively. Such appropriate gaps are attributed to the dominant Ni $3d$ orbital contribution in the vicinity of the Fermi level. Furthermore, we also calculated parity eigenvalues at the time-reversal invariant momenta (TRIM) points (see details in Table S1 [43]). For the cubic system, there are eight invariant momenta (Γ, $3X$, $3M$, R), including a Γ point, a R point, three inequivalent X points, and three inequivalent M points. The $\mathbb{Z}_2$ invariants are determined as (0;111) by parity analysis. These results indicate that the nontrivial nodal-line semimetal transforms into a topological insulator with a weak $\mathbb{Z}_2$ index from the effect of SOC. The occupied and unoccupied states have the same topological $\mathbb{Z}_2$ indexes in the case of ignoring SOC, and thus the topologically nontrivial characterization agrees with the existence of Dirac nodal rings [8].

Generally, such topological nodal rings have nontrivial surface states. As expected, one can see that nontrivial surface bands emerge on the (001) surface shown in Fig. 6, although the surface states are mixed with the bulk states, which obscures the existence of topological characterization. At the $\bar{M}$ points, the surface band can connect with Dirac cones. There are clear Fermi arcs along the $\bar{M}$-$\bar{\Gamma}$ and $\bar{X}$-$\bar{\Gamma}$ high-symmetry paths on the corresponding projected (001) surface (see Fig. 6).

IV. CONCLUSION

In conclusion, we have investigated the evolution of band structures of Ni_3In-based compounds. When the lattice symmetry is constrained, we can control the topological states and the position of nodal lines by fine-tuning the composition. By controlling the proper ratio of intercalated atoms, we realize the ideal nodal-line fermions in $Ni_3InC_{0.26}N_{0.74}$, which would be feasible in experiments, and thus our work provides a promising avenue to explore ideal nodal lines in doped systems. Our charge analysis indicates that the bond interaction between intercalated atoms and nickel atoms induces charge redistribution, giving rise to the rigidlike shift of bands. Moreover, this nontrivial state is insensitive to applied strain and pressure, so one can expect exotic correlation physics of massless nodal-line fermions in doped structures.

ACKNOWLEDGMENTS

This work was supported by the National Natural Science Foundation of China (Grants No. 12204449, No. 11888101, No. 12222402, and No. 12347101), the China Postdoctoral

Science Foundation (Grant No. 2022M723068), the Anhui Initiative in Quantum Information Technologies (Grant No. AHY160000), the Key Research Program of Frontier Sciences, CAS, China (Grant No. QYZDYSSWSLH021), and the National Key Research and Development Program of the Ministry of Science and Technology of China (Grants No. 2019YFA0704901 and No. 2016YFA0300201). The DFT calculations in this work are supported by the Beijing Super Cloud Computing Center (BSCC) and the Supercomputing Center of University of Science and Technology of China.

[1] X. Wan, A. M. Turner, A. Vishwanath, and S. Y. Savrasov, Topological semimetal and Fermi-arc surface states in the electronic structure of pyrochlore iridates, Phys. Rev. B **83**, 205101 (2011).

[2] Z. Wang, Y. Sun, X.-Q. Chen, C. Franchini, G. Xu, H. Weng, X. Dai, and Z. Fang, Dirac semimetal and topological phase transitions in A_3Bi (A = Na, K, Rb), Phys. Rev. B **85**, 195320 (2012).

[3] Z. K. Liu, B. Zhou, Y. Zhang, Z. J. Wang, H. M. Weng, D. Prabhakaran, S.-K. Mo, Z. X. Shen, Z. Fang, X. Dai, Z. Hussain, and Y. L. Chen, Discovery of a three-dimensional topological Dirac semimetal, Na_3Bi, Science **343**, 864 (2014).

[4] S.-Y. Xu, C. Liu, S. K. Kushwaha, R. Sankar, J. W. Krizan, I. Belopolski, M. Neupane, G. Bian, N. Alidoust, T.-R. Chang, H.-T. Jeng, C.-Y. Huang, W.-F. Tsai, H. Lin, P. P. Shibayev, F.-C. Chou, R. J. Cava, and M. Z. Hasan, Observation of Fermi arc surface states in a topological metal, Science **347**, 294 (2015).

[5] Z. Wang, H. Weng, Q. Wu, X. Dai, and Z. Fang, Three-dimensional Dirac semimetal and quantum transport in Cd_3As_2, Phys. Rev. B **88**, 125427 (2013).

[6] Q. Wang, Y. Xu, R. Lou, Z. Liu, M. Li, Y. Huang, D. Shen, H. Weng, S. Wang, and H. Lei, Large intrinsic anomalous Hall effect in half-metallic ferromagnet $Co_3Sn_2S_2$ with magnetic Weyl fermions, Nat. Commun. **9**, 3681 (2018).

[7] B. Q. Lv, H. M. Weng, B. B. Fu, X. P. Wang, H. Miao, J. Ma, P. Richard, X. C. Huang, L. X. Zhao, G. F. Chen, Z. Fang, X. Dai, T. Qian, and H. Ding, Experimental discovery of Weyl semimetal TaAs, Phys. Rev. X **5**, 031013 (2015).

[8] Y. Kim, B. J. Wieder, C. L. Kane, and A. M. Rappe, Dirac line nodes in inversion-symmetric crystals, Phys. Rev. Lett. **115**, 036806 (2015).

[9] H. Weng, C. Fang, Z. Fang, B. A. Bernevig, and X. Dai, Weyl semimetal phase in noncentrosymmetric transition-metal monophosphides, Phys. Rev. X **5**, 011029 (2015).

[10] L. M. Schoop, M. N. Ali, C. Straßer, A. Topp, A. Varykhalov, D. Marchenko, V. Duppel, S. S. Parkin, B. V. Lotsch, and C. R. Ast, Dirac cone protected by non-symmorphic symmetry and three-dimensional Dirac line node in ZrSiS, Nat. Commun. **7**, 11696 (2016).

[11] T. Bzdusek, Q. Wu, A. Ruegg, M. Sigrist, and A. A. Soluyanov, Nodal-chain metals, Nature (London) **538**, 75 (2016).

[12] Q. Xu, R. Yu, Z. Fang, X. Dai, and H. Weng, Topological nodal line semimetals in the CaP_3 family of materials, Phys. Rev. B **95**, 045136 (2017).

[13] A. A. Burkov, M. D. Hook, and L. Balents, Topological nodal semimetals, Phys. Rev. B **84**, 235126 (2011).

[14] C. Fang, H. Weng, X. Dai, and Z. Fang, Topological nodal line semimetals, Chin. Phys. B **25**, 117106 (2016).

[15] B. Q. Lv, T. Qian, and H. Ding, Experimental perspective on three-dimensional topological semimetals, Rev. Mod. Phys. **93**, 025002 (2021).

[16] X. Zhao, P.-j. Guo, F. Ma, and Z.-Y. Lu, Coexistence of topological Weyl and nodal-ring states in ferromagnetic and ferrimagnetic double perovskites, Phys. Rev. B **103**, 085138 (2021).

[17] N. B. Kopnin, T. T. Heikkilä, and G. E. Volovik, High-temperature surface superconductivity in topological flat-band systems, Phys. Rev. B **83**, 220503(R) (2011).

[18] Y. Huh, E.-G. Moon, and Y. B. Kim, Long-range Coulomb interaction in nodal-ring semimetals, Phys. Rev. B **93**, 035138 (2016).

[19] S. Xue, M. Wang, Y. Li, S. Zhang, X. Jia, J. Zhou, Y. Shi, X. Zhu, Y. Yao, and J. Guo, Observation of nodal-line plasmons in ZrSiS, Phys. Rev. Lett. **127**, 186802 (2021).

[20] W. Duan, J. Zhang, R. Kumar, H. Su, Y. Zhou, Z. Nie, Y. Chen, M. Smidman, C. Cao, Y. Song, and H. Yuan, Nodeless superconductivity in the topological nodal-line semimetal $CaSb_2$, Phys. Rev. B **106**, 214521 (2022).

[21] L. Chen, C. Setty, H. Hu, M. G. Vergniory, S. E. Grefe, L. Fischer, X. Yan, G. Eguchi, A. Prokofiev, S. Paschen, J. Cano, and Q. Si, Topological semimetal driven by strong correlations and crystalline symmetry, Nat. Phys. **18**, 1341 (2022).

[22] J.-W. Rhim and Y. B. Kim, Landau level quantization and almost flat modes in three-dimensional semimetals with nodal ring spectra, Phys. Rev. B **92**, 045126 (2015).

[23] S. T. Ramamurthy and T. L. Hughes, Quasitopological electromagnetic response of line-node semimetals, Phys. Rev. B **95**, 075138 (2017).

[24] K. Kim, J. Seo, E. Lee, K.-T. Ko, B. S. Kim, B. G. Jang, J. M. Ok, J. Lee, Y. J. Jo, W. Kang, J. H. Shim, C. Kim, H. W. Yeom, B. I. Min, B.-J. Yang, and J. S. Kim, Large anomalous Hall current induced by topological nodal lines in a ferromagnetic van der Waals semimetal, Nat. Mater. **17**, 794 (2018).

[25] H. Wang, J. Ruan, and H. Zhang, Non-Hermitian nodal-line semimetals with an anomalous bulk-boundary correspondence, Phys. Rev. B **99**, 075130 (2019).

[26] Z. Zhu, H. Liu, Y. Ge, Z. Zhang, W. Wu, C. Xiao, and S. A. Yang, Third-order charge transport in a magnetic topological semimetal, Phys. Rev. B **107**, 205120 (2023).

[27] B. Sohn, E. Lee, S. Y. Park, W. Kyung, J. Hwang, J. D. Denlinger, M. Kim, D. Kim, B. Kim, H. Ryu, S. Huh, J. S. Oh, J. K. Jung, D. Oh, Y. Kim, M. Han, T. W. Noh, B.-J. Yang, and C. Kim, Sign-tunable anomalous Hall effect induced by two-dimensional symmetry-protected nodal structures in ferromagnetic perovskite thin films, Nat. Mater. **20**, 1643 (2021).

[28] R. Yu, H. Weng, Z. Fang, X. Dai, and X. Hu, Topological node-line semimetal and Dirac semimetal state in antiperovskite Cu_3PdN, Phys. Rev. Lett. **115**, 036807 (2015).

[29] G. Bian, T.-R. Chang, R. Sankar, S.-Y. Xu, H. Zheng, T. Neupert, C.-K. Chiu, S.-M. Huang, G. Chang, I. Belopolski, D. S. Sanchez, M. Neupane, N. Alidoust, C. Liu, B. Wang, C.-C. Lee, H. T. Jeng, C. Zhang, Z. Yuan, S. Jia *et al.*, Topological

nodal-line fermions in spin-orbit metal $PbTaSe_2$, Nat. Commun. **7**, 10556 (2016).

[30] G. Bian, T. R. Chang, H. Zheng, S. Velury, S. Y. Xu, T. Neupert, C.-K. Chiu, S.-M. Huang, D. S. Sanchez, I. Belopolski, N. Alidoust, P.-J. Chen, G. Chang, A. Bansil, H.-T. Jeng, H. Lin, and M. Z. Hasan, Drumhead surface states and topological nodal-line fermions in $TlTaSe_2$, Phys. Rev. B **93**, 121113(R) (2016).

[31] B. Feng, B. Fu, S. Kasamatsu, S. Ito, P. Cheng, C.-C. Liu, Y. Feng, S. Wu, S. K. Mahatha, P. Sheverdyaeva, P. Moras, M. Arita, O. Sugino, T.-C. Chiang, K. Shimada, K. Miyamoto, T. Okuda, K. Wu, L. Chen, Y. Yao *et al.*, Experimental realization of two-dimensional Dirac nodal line fermions in monolayer Cu_2Si, Nat. Commun. **8**, 1007 (2017).

[32] X. Li, J. Koo, Z. Zhu, K. Behnia, and B. Yan, Field-linear anomalous Hall effect and Berry curvature induced by spin chirality in the kagome antiferromagnet Mn_3Sn, Nat. Commun. **14**, 1642 (2023).

[33] C. Fang, Y. Chen, H.-Y. Kee, and L. Fu, Topological nodal line semimetals with and without spin-orbital coupling, Phys. Rev. B **92**, 081201(R) (2015).

[34] T. Bzdušek and M. Sigrist, Robust doubly charged nodal lines and nodal surfaces in centrosymmetric systems, Phys. Rev. B **96**, 155105 (2017).

[35] W. Kohn and L. J. Sham, Self-consistent equations including exchange and correlation effects, Phys. Rev. **140**, A1133 (1965).

[36] G. Kresse and J. Furthmüller, Efficient iterative schemes for *ab initio* total-energy calculations using a plane-wave basis set, Phys. Rev. B **54**, 11169 (1996).

[37] J. P. Perdew, K. Burke, and M. Ernzerhof, Generalized gradient approximation made simple, Phys. Rev. Lett. **77**, 3865 (1996).

[38] H. J. Monkhorst and J. D. Pack, Special points for Brillouin-zone integrations, Phys. Rev. B **13**, 5188 (1976).

[39] J. Gao, Q. Wu, C. Persson, and Z. Wang, IRVSP: To obtain irreducible representations of electronic states in the VASP, Comput. Phys. Commun. **261**, 107760 (2021).

[40] A. A. Mostofi, J. R. Yates, Y.-S. Lee, I. Souza, D. Vanderbilt, and N. Marzari, WANNIER90: A tool for obtaining maximally-localised Wannier functions, Comput. Phys. Commun. **178**, 685 (2008).

[41] Q. Wu, S. Zhang, H.-F. Song, M. Troyer, and A. A. Soluyanov, WANNIERTOOLS: An open-source software package for novel topological materials, Comput. Phys. Commun. **224**, 405 (2018).

[42] A. Togo, L. Chaput, T. Tadano, and I. Tanaka, Implementation strategies in PHONOPY and PHONO3PY, J. Phys.: Condens. Matter. **35**, 353001 (2023).

[43] See Supplemental Material at http://link.aps.org/supplemental/10.1103/PhysRevB.109.205103 for the topological $\mathbb{Z}_2$ invariants, phonon spectrum electron localization function, and tunable band strutures under different approaches for the Ni_3InX compounds.

[44] S. Liu, Y. Yang, F. Yu, X. Wen, Z. Gui, K. Peng, R. Wang, and J. Ying, Pressure-induced superconductivity and nontrivial band topology in compressed γ-InSe, Phys. Rev. B **105**, 214506 (2022).

[45] Y. Yang, F. Yu, X. Wen, Z. Gui, Y. Zhang, F. Zhan, R. Wang, J. Ying, and X. Chen, Pressure-induced transition from a Mott insulator to a ferromagnetic Weyl metal in $La_2O_3Fe_2Se_2$, Nat. Commun. **14**, 2260 (2023).

[46] H. Weng, X. Dai, and Z. Fang, Transition-metal pentatelluride $ZrTe_5$ and $HfTe_5$: A paradigm for large-gap quantum spin Hall insulators, Phys. Rev. X **4**, 011002 (2014).

[47] H. Yang, S. W. Kim, M. Chhowalla, and Y. H. Lee, Structural and quantum-state phase transitions in van der Waals layered materials, Nat. Phys. **13**, 931 (2017).

[48] K.-H. Jin, H. W. Yeom, and F. Liu, Doping-induced topological phase transition in Bi: The role of quantum electronic stress, Phys. Rev. B **101**, 035111 (2020).